JOURNAL OF COMPUTATIONAL PHYSICS 103, 116–125 (1992)

Radiation-Induced Cavitation Process in a Metastable Superheated Liquid

I. Initial and Pre-bubble Formation Stages

Y. Y. SUN, B. T. CHU, AND R. E. APFEL

Department of Mechanical Engineering, Yale University, New Haven, Connecticut 06520

Received September 15, 1989; revised December 13, 1990

The cavitation phenomenon in a superheated liquid following the irradiation of the medium by a flux of neutrons is studied from a macroscopic viewpoint. This is, essentially, the bubble chamber problem. The interaction between the neutron flux with the material medium is modeled here as a sudden deposition of energy along a straight line in a medium which may undergo phase transition. Mathematically the problem consists of solving the nonlinear fluid dynamic equations governing the motion of a viscous, heat-conducting, compressible fluid subjected to the singular initial condition of a sudden energy deposition along an infinite line. Time evolution of the resulting "thermal spike" and cylindrical shock wave produced is followed by numerical computations. A scaling transformation is used to resolve the initial development of the singularity. The leading term in the solution at the initial stage is in agreement with the solution which may be inferred by dimensional reasoning and obtained by the similarity method. Subsequent development of the flow field is first followed by the implicit donor-cell finite difference method and then by Miller's moving finite element method, to account for the multiple propagating steep gradients developed in the course of time. The necessity of using a combination of numerical and analytical techniques to solve such a complex problem is discussed. Part I of this paper is concerned with the development of the flow field leading to the incipient formation of an "embryonic" bubble. Part II discusses the growth of this "embryonic" bubble leading to cavitation or to its eventual collapse.

1. INTRODUCTION

Moderately superheated drops of liquid will be vaporized when exposed to sufficiently intense neutron radiation. The process can be explained from both the microscopic and macroscopic viewpoints.

From a microscopic viewpoint, the radiation-induced cavitation process is a neutron–nucleus interaction process. This interaction results in the nucleation and growth of an "embryonic" bubble in the medium leading to the cavitation phenomenon. This process begins with the interaction of a neutron with one of the atoms of the superheated liquid. As a result, the agitated ion begins to shuttle through the liquid and imparts its energy to the molecules in the liquid. Again, the highly agitated molecules around the ion track interact with their neighboring molecules, imparting to the latter some of their energies. Such interaction propagates radially outward from the ion path, resulting in the observation of a rapidly expanding region of extremely hot fluid. This is the thermal spike envisioned by Seitz [10, 11].

From the macroscopic viewpoint, the process may be divided into the following stages: (1) *The initial stage.* Energy is deposited locally in a very small region producing a localized region of high temperature, referred to above as a "thermal spike." The sudden expansion of this intensely thermalized region produces a strong shock wave propagating outward into the surrounding medium. In the initial stage, the temperature T and pressure p of the fluid within the shock enclosure far exceed the critical temperature T_c and the critical pressure p_c. There is no distinction between liquid and vapor, and there cannot be any "bubble." (2) *The pre-bubble formation stage or "cooling stage."* As the energy is transmitted from the thermalized region to the surrounding medium through shock propagation and heat conduction, the temperature and pressure of the fluid within the shock enclosure decrease, the expansion process slows down and the shock wave decays. (3) *The interface formation stage.* The vapor–liquid interface will be formed at some radial distance when T and p reach the critical temperature and pressure giving rise to an "embryonic" bubble. (4) *The post-interface formation stage* or *developing stage.* If the energy deposited in the medium is sufficiently high, the vapor cavity enclosed with the "embryonic" bubble will grow indefinitely; if the energy is not high enough, then the growth of the cavity may be impeded by the interfacial and viscous forces as well as by conduction heat lost, to such an extent that the bubble may in the end collapse and there is no cavitation.

In this paper, the radiation-induced cavitation process will be studied from the macroscopic viewpoint. Several problems are of special interest such as the threshold energy required for "cavitation," the calculation, and the descrip-

0021-9991/92 $5.00

tion of the radiation-induced cavitation process and the flow fields at different stages. Radiation-induced cavitation can be detected by acoustic methods such as *superheated drop detectors* (SDD) invented by Apfel [1, 2], but the details of the process and the flow fields are difficult to measure. The difficulty arises principally from the extremely small length and time scales on which these phenomena take place in nature (for details and numerical values, see Section 6, Part 2). We propose to construct a mathematical theory to describe the ongoing complex process and attempt to predict the outcome with numerical calculations. Two assumptions will be made: (1) The behavior of the medium can be described by the usual macroscopic fluid equations. It follows that the flow fields can be described by the general fluid dynamic equations which form a nonlinear partial differential equation (PDE) system; (2) Energy is deposited uniformly along an infinite line. These two assumptions are probably acceptable up to the formation of a critical size cavity.

There are some special difficulties in solving this PDE system related to the radiation-induced cavitation process: (1) Singularity at the initial stage referred to as the "thermal spike"; (2) The emergence of a second phase leading to rapid changes in the coefficients of viscosities, thermal conductivities, densities, specific heats, etc.; (3) Multiple moving steep gradients such as the propagating shock wave and vapor–liquid interface.

A hybrid methodology is designed to overcome the above difficulties and to solve the following problems:

(1) When energy is suddenly deposited at a point, line, or plane in a perfect gas, it is well known that the initial development of the flow is self-similar [3, 7]. This result is found to be also true for real fluids which may exhibit phase transformation. The scaling transformation is used to overcome the singularity difficulty and to establish the initial flow field as the initial conditions of the whole process. The partial differential equations reduce to an ordinary differential equation system (ODE) using the scaling transformation normalized by the shock radius R and the shock speed $\dot{R}$. This ODE system can be solved by the predictor–corrector method and the shooting method. The above methods can only be used to compute the flow fields for a few time steps, since the simple shooting method is an unstable method.

(2) The implicit donor-cell finite difference method (FDM) is used to solve the flow field at the pre-bubble formation stage with the same variables as in the scaling transformation. The extrapolation using the information of the three previous time steps is adopted to calculate the first guess of Newton iteration. The flow fields at $t=0$, $t=\Delta t$, and $t=2\,\Delta t$ are supplied by the above scaling transformation analysis. As time evolves, density gradients become steeper and steeper. Since the implicit donor-cell FDM is a fixed grid method, it can no longer be adapted to the moving steep gradients when phase change is about to occur somewhere. Hence, adaptive computational methods are introduced.

Part I of this paper is concerned with the flow development and physical changes occurring in the initial stage and the pre-bubble formation stage mentioned above.

(3) Miller's moving finite element method (MFEM) is used to solve the flow fields of the interface formation stage and the post-interface formation stage with multiple moving steep gradients. The flow field solved by the implicit donor-cell FDM is used as the initial conditions of the MFEM. It is not advisable to connect the MFEM directly with the similarity solution for two reasons: (1) The magnitudes of the various physical variables change by many orders of magnitude between the initial phase of flow development and the subsequent stages of bubble growth or collapse. (2) The physical scale is extremely small in terms of L, the length scale characterizing the phenomena. The same problem does not occur with the FDM, because the length scale is normalized by the shock radius which is itself very small in the initial stage of development and because similarity variables instead of the physical variables are used in the formulation of FDM. If the MFEM were connected directly to the similarity solution, the rapid decrease of various physical variables in the initial phase of pre-bubble formation stage would require extremely small time steps to resolve the changes. Consequently, the inclusion of the solution of the implicit donor-cell FDM for intermediate times is important. Part II will cover the MFEM and deal with bubble formation and its evolution with time.

2. GOVERNING EQUATIONS

Under the assumptions made, the fluid motion can be described by the usual macroscopic fluid equations. The flow field is governed by a system of five equations, namely, three conservation equations (mass, momentum, and energy conservation), one equation of state, and one specific internal energy equation. They are sufficient to solve for the five unknowns: temperature T, pressure p, velocity u, specific volume v (density $\rho = 1/v$), and specific internal energy e. The medium is modeled by a Horvath–Lin fluid [5].

In a cylindrical coordinate system, the mass, momentum, and energy conservation equations are

$$\frac{\partial \rho}{\partial t} + \frac{1}{r}\frac{\partial (\rho r u)}{\partial r} = 0, \tag{1}$$

$$\rho\left(\frac{\partial u}{\partial t} + u\frac{\partial u}{\partial r}\right) = \rho f_r - \frac{\partial p}{\partial r} + \frac{4}{3}\mu\frac{\partial}{\partial r}\left[\frac{1}{r}\frac{\partial (ur)}{\partial r}\right] + \frac{4}{3}\frac{\partial \mu}{\partial r}\left[\frac{\partial u}{\partial r} - \frac{1}{2}\frac{u}{r}\right], \tag{2}$$

and

$$\rho c_v\left(\frac{\partial T}{\partial t}+u\frac{\partial T}{\partial r}\right)+Tp_T\left(\frac{\partial u}{\partial r}+\frac{u}{r}\right)$$
$$=\frac{4}{3}\mu\left[\frac{1}{r}\frac{\partial(ur)}{\partial r}\right]^2-4\mu\frac{u}{r}\frac{\partial u}{\partial r}+\frac{1}{r}\frac{\partial}{\partial r}\left(\kappa r\frac{\partial T}{\partial r}\right)+\rho q, \quad (3)$$

where t denotes time and r is the radial distance; μ, κ, and c_v are respectively the viscosity, thermal conductivity, and specific heat capacity at constant volume of the fluid, f_r is body force and $P_T=(\partial P/\partial T)_v$.

The thermal equation of state will be modeled by the Horvath–Lin equation

$$p=\frac{R^*T}{v-b}-\frac{a}{Tv(v+c)}, \quad (4)$$

where a, b, and c are three parameters in Horvath–Lin's equation. R^* is the gas constant.

The specific internal energy equation associated with the Horvath–Lin's equation is

$$e=e_0+\int_{T_0}^{T}c_{v,\text{ideal}}(T)\,dT+\frac{2a}{cT}\ln\left(\frac{v}{v+c}\right)$$
$$-\frac{2a}{cT_0}\ln\left(\frac{v_0}{v_0+c}\right), \quad (5)$$

where e_0, T_0, and v_0 are the undisturbed values of e, T, and v, respectively.

The boundary conditions at $r=0$ are

$$u=0, \quad (6)$$

$$\frac{\partial T}{\partial r}=0. \quad (7)$$

From the momentum conservation equation (suppose $f_r=0$), and $\mathbf{u}=0$ at $\mathbf{r}=0$, we have the third boundary condition at $r=0$:

$$\frac{4}{3}\mu\frac{\partial}{\partial r}\left[\frac{1}{r}\frac{\partial}{\partial r}(ur)\right]=\frac{\partial p}{\partial r}. \quad (8)$$

The boundary conditions as $r\to\infty$ are

$$u=0, \quad (9)$$

$$T=T_0, \quad (10)$$

$$v=v_0. \quad (11)$$

The global energy conservation equation is

$$2\pi\int_0^\infty[\rho(e+\tfrac{1}{2}u^2)-\rho_0e_0]\,r\,dr=\bar{E}, \quad (12)$$

where $\bar{E}$ is the energy deposited per unit length.

3. FLOW FIELD IN THE INITIAL STAGE

In the initial stage, energy is deposited locally in an extremely small region, producing a localized region of high temperature. The sudden expansion of this intensely thermalized region produces a strong shock wave, propagating outward into the surrounding medium. As expected, the shock speed $\dot{R}$, velocity u, pressure p, temperature T, and the specific internal energy e approach infinity as the shock radius $R\to 0$. The characteristic feature of the solutions in this stage is its initial behavior. Obviously, it would be impossible to carry out numerical solutions of the boundary value problem in terms of the physical variables. A scaling transformation is introduced to overcome the singularity difficulty.

The size of the above-mentioned small region which expands rapidly with time may be characterized by the shock radius $R(t)$. The exact value of $R(t)$ at any instant t must, of course, be computed. Assuming this is known for the moment, the expansion rate of the highly thermalized region may be characterized by the shock speed $\dot{R}(t)$. It is easy to see that $\dot{R}\to\infty$ as $R\to 0$, cf. Eq. (13d) below. From the shock wave theory, u is of the order of $\dot{R}$; $e-e_0$ is of the order of $\dot{R}^2$ as $R\to 0$; p, of the order of $\rho_0\dot{R}^2$; T, of the order of $\dot{R}^2/R^*$ (R^* is the gas constant); ρ and v are both of order unity as $R\to 0$. It is, therefore, imperative to renormalize the dependent variables so that they remain bounded within the shock enclosure as $R\to 0$ (i.e., immediately following the energy deposition). To this end, let us introduce the dimensionless variables,

$$\bar{u}=\frac{u}{\dot{R}}, \quad \bar{e}=\frac{e-e_0}{\dot{R}^2}, \quad \bar{p}=\frac{p}{\rho_0\dot{R}^2}, \quad (13a)$$

$$\bar{T}=\frac{R^*T}{\dot{R}^2}, \quad \bar{\rho}=\frac{\rho}{\rho_0}, \quad \bar{v}=\frac{v}{v_0}, \quad (13b)$$

and

$$\bar{x}=\frac{r}{R(t)}, \quad \bar{R}=\frac{R}{L}, \quad V_s=\frac{\dot{R}}{(R^*T_0)^{1/2}}$$
$$\bar{c}_{\bar{v}}=\frac{c_v}{R^*}, \quad \bar{\mu}=\frac{\mu}{\rho_0}\left(\frac{\bar{E}}{\pi\rho_0}\right)^{-1/2}, \quad (13c)$$
$$\bar{\chi}=\frac{\chi}{L(R^*T_0)^{1/2}},$$

where

$$L=\left(\frac{\bar{E}}{\pi\rho_0R^*T_0}\right)^{1/2},$$
$$\bar{E}=2\pi\rho_0R^2\dot{R}^2\int_0^1\bar{x}\,d\bar{x}\left(\bar{e}+\frac{1}{2}\bar{u}^2\right)\Big/\bar{v}, \quad (13d)$$
$$\chi=\frac{\kappa}{\rho R^*}, \quad \phi_0=\frac{p_0}{\rho_0R^*T_0}.$$

Here, L is a characteristic length which is of the order of the radius of a column of original fluid of unit length having a total energy $\bar{E}$, and V_s is the dimensionless shock speed; $\bar{c}_{\bar{v}}$, $\bar{\mu}$, $\bar{\chi}$, and ϕ_0 are respectively the dimensionless specific heat, viscosity, thermal diffusivity, and compressibility factor $(p_0 v_0/R^* T_0)$. Finally, $\bar{x}$ and $\bar{R}$ are the dimensionless radial distance and the shock radius. In the initial stage and the pre-bubble formation stage, it is convenient to regard $\bar{R}$ as a measure of time t elapsed since the energy deposition. Since the shock radius R and time t are related by $t = \int_0^R (dR/R)$ with the shock speed $\dot{R}$ as a function of R determined as part of the solution, the dimensionless $\bar{R}$ will be related to the dimensionless time $\bar{t}$ defined as

$$\bar{t} = t \frac{(R^* T_0)^{1/2}}{L} \tag{14a}$$

by the equation

$$\bar{t} = \int_0^{\bar{R}} \frac{d\bar{R}}{V_s} \tag{14b}$$

or

$$\bar{t} = \int_0^{\bar{R}} \Gamma(\bar{R})\, \bar{R}\, d\bar{R}, \tag{14c}$$

where Γ, defined by

$$\Gamma = \frac{1}{V_s \bar{R}}, \tag{15}$$

remains finite as $\bar{R} \to 0$, cf. Eq. (13d).

With $\bar{R}$ and $\bar{x}$ as the independent variables, instead of t and x, and subscripts $\bar{R}$ and $\bar{x}$ as the partial derivatives with respect to indicated variables, the governing equations (1)–(5) can be rewritten in the dimensionless form

$$\bar{R}\bar{v}_{\bar{R}} + (\bar{u} - \bar{x})\, \bar{v}_{\bar{x}} - \bar{v}(\bar{u}_{\bar{x}} + \bar{u}/\bar{x}) = 0, \tag{16}$$

$$\bar{R}\bar{u}_{\bar{R}} + (\bar{u} - \bar{x})\, \bar{u}_{\bar{x}} - \bar{u} - \bar{u}\bar{R}(\ln \Gamma)_{\bar{R}} = -\bar{v}\bar{p}_{\bar{x}} + \frac{4}{3}\frac{\bar{\mu}\Gamma}{\bar{\rho}}\left[\frac{1}{\bar{x}}(\bar{u}\bar{x})_{\bar{x}}\right]_{\bar{x}} + \frac{4}{3}\frac{\Gamma}{\bar{\rho}}\bar{\mu}_{\bar{x}}\left(\bar{u}_{\bar{x}} - \frac{1}{2}\frac{\bar{u}}{\bar{x}}\right), \tag{17}$$

$$\bar{R}\bar{e}_{\bar{R}} + (\bar{u} - \bar{x})\, \bar{e}_{\bar{x}} - 2\bar{e}(1 + \dot{\bar{R}}(\ln \Gamma)_{\bar{R}}) + \bar{p}\bar{v}(\bar{u}_{\bar{x}} + \bar{u}/\bar{x}) = \bar{v}\Gamma[(\bar{\chi}\bar{T}_{\bar{x}})_{\bar{x}} + (\bar{\chi}\bar{T}_{\bar{x}})/\bar{x}] + \frac{4}{3}\Gamma\bar{v}\bar{\mu}\left[\frac{1}{\bar{x}}(\bar{u}\bar{x})_{\bar{x}}\right]^2 - 4\Gamma\bar{v}\bar{\mu}\frac{\bar{u}}{\bar{x}}\bar{u}_{\bar{x}}, \tag{18}$$

$$\bar{p} = \frac{\bar{T}}{\bar{v} - \beta_h} - \frac{1}{\bar{T}}\frac{\alpha_h}{\bar{v}(\bar{v} + \gamma_h)}\Gamma^4 \bar{R}^4, \tag{19}$$

and

$$\bar{e} = \int_{\Gamma^2\bar{R}^2}^{\bar{T}} \bar{c}_{\bar{v},\,\text{ideal}}\left(\frac{T_0\tau}{\Gamma^2\bar{R}^2}\right) d\tau + \frac{2\alpha_h}{\gamma_h}\Gamma^2\bar{R}^2 \ln(1 + \gamma_h) + \frac{2\alpha_h}{\gamma_h}\frac{\Gamma^4\bar{R}^4}{\bar{T}} \ln\left(\frac{\bar{v}}{\bar{v} + \gamma_h}\right), \tag{20}$$

where the new dimensionless parameters α_h, β_h, and γ_h are related to the parameters a, b, and c of the Horvath–Lin's equation of state by

$$\alpha_h = \frac{aR^*}{v_0(R^* T_0)^2}, \qquad \beta_h = \frac{b}{v_0}, \qquad \gamma_h = \frac{c}{v_0}. \tag{21}$$

Now we shall introduce a number of simplifying assumptions: (1) the fluid medium ahead of the shock front may be assumed inviscid and non-conductive; (2) the viscosity and conductivity within the shock enclosure are constant. Admittedly, the latter assumption is extremely crude, since there is a large temperature variation in the flow field, especially in the initial stage of flow development. Fortunately, as our computation results will indicate, viscosity assumes a rather minor role in the initial stage of flow development behind the shock enclosure. The same, however, cannot be said of heat conductivity.

The boundary conditions at $\bar{x} = 1$ are the conservation relationships

$$\bar{u} = 1 - \bar{v},$$
$$\bar{p} = 1 - \bar{v} + \phi_0\Gamma^2\bar{R}^2 - \frac{2}{3}\bar{\mu}\Gamma\left(\frac{\bar{u}}{\bar{x}} - 2\bar{u}_{\bar{x}}\right), \tag{22}$$
$$\bar{e} = \frac{1}{2}(1 - \bar{v})^2 - \Gamma\bar{\chi}\bar{T}_{\bar{x}}, + \phi_0\Gamma^2\bar{R}^2(1 - \bar{v}),$$

while the global energy equation, expressed in terms of the new variables, assumes the form

$$\Gamma^2 = 2\int_0^1 \bar{x}\, d\bar{x}(\bar{e} + \bar{u}^2/2)/\bar{v}. \tag{23}$$

Define $\bar{q}$, $\bar{B}$, and $\bar{W}$ by

$$\bar{q} = \bar{T}_{\bar{x}}\bar{\chi},$$
$$\bar{B} = 2\int_0^{\bar{x}} \bar{x}\, d\bar{x}\, \frac{(\bar{e} + \bar{u}^2/2)}{\bar{v}}, \tag{24}$$
$$\bar{W} = \bar{u}_{\bar{x}}.$$

Regarding $\bar{R}$ as a parameter, the system of equations can be cast in a form of an ODE system:

$$\frac{d\bar{v}}{d\bar{x}}=\left[\frac{\bar{u}^2}{\bar{x}}-\bar{v}\bar{p}_{\bar{T}}\bar{T}_{\bar{x}}-\bar{R}\left[\bar{u}_{\bar{R}}+\frac{\bar{v}_{\bar{R}}}{\bar{v}}(\bar{u}-\bar{x})-\bar{u}(\ln\Gamma)_{\bar{R}}\right]+VA\right]\times\frac{\bar{v}}{(\bar{u}-\bar{x})^2+\bar{v}^2\bar{p}_{\bar{v}}+VB}, \tag{25}$$

$$\frac{d\bar{u}}{d\bar{x}}=(\bar{u}-\bar{x})\frac{\bar{v}_{\bar{x}}}{\bar{v}}-\frac{\bar{u}}{\bar{x}}+\bar{R}\frac{\bar{v}_{\bar{R}}}{\bar{v}}, \tag{26}$$

$$\frac{d\bar{W}}{d\bar{x}}=-\frac{3\bar{\rho}}{4\bar{\mu}\Gamma}\left[\left[(\bar{u}-\bar{x})-\frac{4\bar{\mu}\Gamma}{3\rho}\left(\frac{1}{\bar{x}}+(\ln\bar{\mu})_{\bar{x}}\right)\right](\bar{u}-\bar{x})+\bar{v}^2\bar{p}_{\bar{v}}\right]\frac{\bar{v}_{\bar{x}}}{\bar{v}}+\frac{3\bar{\rho}}{4\bar{\mu}\Gamma}\left[\frac{\bar{u}^2}{\bar{x}}-\bar{v}\bar{p}_{\bar{T}}\bar{T}_{\bar{x}}-\bar{R}\left[\bar{u}_{\bar{R}}+\frac{(\bar{u}-\bar{x})}{\bar{v}}\bar{v}_{\bar{R}}-\bar{u}(\ln\Gamma)_{\bar{R}}\right]\right]+\frac{\bar{R}\bar{v}_{\bar{R}}}{\bar{x}\bar{v}}+(\ln\bar{\mu})_{\bar{x}}\left(\frac{\bar{R}\bar{v}_{\bar{R}}}{\bar{v}}-\frac{\bar{u}}{2\bar{x}}\right), \tag{27}$$

$$\frac{d\bar{T}}{d\bar{x}}=\frac{\bar{q}}{\bar{\chi}}, \tag{28}$$

$$\frac{d\bar{q}}{d\bar{x}}=-\frac{\bar{q}}{\bar{x}}+\frac{1}{\bar{v}\Gamma}[\bar{R}[\bar{e}_{\bar{R}}]+(\bar{u}-\bar{x})[\bar{e}_{\bar{x}}]-2[\bar{e}](1+\bar{R}(ln\,\Gamma)_{\bar{R}})+\bar{p}\bar{v}(\bar{u}_{\bar{x}}+\bar{u}/\bar{x})]-\frac{4}{3}\bar{\mu}\left[\left(\frac{\bar{u}}{\bar{x}}+\bar{u}_{\bar{x}}\right)^2+3\frac{\bar{u}}{\bar{x}}\bar{u}_{\bar{x}}\right], \tag{29}$$

$$\frac{d\bar{B}}{d\bar{x}}=\frac{2\bar{x}(\bar{e}+\bar{u}^2/2)}{\bar{v}}. \tag{30}$$

The boundary conditions at $\bar{x}=1$ are

$$\begin{aligned}&\bar{u}=1-\bar{v},\\&\bar{p}=1-\bar{v}+\phi_0\Gamma^2\bar{R}^2-\frac{2}{3}\Gamma\bar{\mu}\left(\frac{\bar{u}}{\bar{x}}-2\bar{u}_{\bar{x}}\right),\\&\bar{e}=\frac{1}{2}(1-\bar{v})^2-\Gamma\bar{q}+\phi_0\Gamma^2\bar{R}^2(1-\bar{v}),\\&\bar{B}=\Gamma^2,\end{aligned} \tag{31}$$

while those at $\bar{x}=0$ are

$$\begin{aligned}&\bar{u}=0,\\&\bar{q}=0,\\&\bar{B}=0,\\&\bar{W}'_{\bar{x}}=0,\end{aligned} \tag{32}$$

[1] This boundary condition can be derived from the continuity equation (1), assuming that ρ is a differentiable function of the spatial coordinates at $r=0$ so that $(\partial/\partial r)(\ln\rho)=0$. Thus, writing Eq. (1) in the form $u=-r[(\partial/\partial t+u(\partial/\partial r))\ln\rho+\partial u/\partial r]$ (Eq. (a)), we conclude that $u(0,t)=0$ for $t>0$, assuming that the derivatives of ρ and u are bounded. Differentiating the above once and letting $r\to 0$, one obtains $(\partial u/\partial r)_{r=0}=-\frac{1}{2}[(\partial/\partial t)(\ln\rho)]_{r=0}$. Differentiating Eq. (a) a second time and letting $r\to 0$, we obtain $(\partial^2u/\partial r^2)_{r=0}=0$. In the normalized system, we have $\bar{W}_{\bar{x}}=0$. Note that in the neighborhood of $r=0$, the velocity behaves like $u=(\partial u/\partial r)_{r=0}r+O(r^3)$ so that $(\partial^2u/\partial r^2)_{r=0}\to 0$. As a result, Eq. (8) could have been replaced by a simpler boundary condition $(\partial p/\partial r)_{r=0}=0$.

where

$$VA=-\frac{4}{3}\frac{\bar{\mu}\Gamma}{\bar{\rho}}\left[\left(\frac{1}{x}+(\ln\bar{\mu})_{\bar{x}}\right)\left(\frac{\bar{u}}{\bar{x}}-\frac{\bar{R}\bar{v}_{\bar{R}}}{\bar{v}}\right)+\bar{W}_{\bar{x}}-\frac{\bar{u}}{\bar{x}^2}-\frac{\bar{u}}{2\bar{x}}(\ln\bar{\mu})_{x}\right], \tag{33}$$

$$VB=-\frac{4}{3}\frac{\bar{\mu}\Gamma}{\bar{\rho}}\left(\frac{1}{\bar{x}}+(\ln\bar{\mu})_{\bar{x}}\right)(\bar{u}-\bar{x}), \tag{34}$$

$$\bar{p}_{\bar{v}}=-\frac{\bar{T}}{(\bar{v}-\beta_h)^2}+\frac{\alpha_h}{\bar{T}}\frac{2\bar{v}+\gamma_h}{\bar{v}^2(\bar{v}+\gamma_h)^2}T^4\bar{R}^4, \tag{35}$$

$$\bar{p}_{\bar{T}}=\frac{1}{(\bar{v}-\beta_h)}+\frac{1}{\bar{T}^2}\frac{\alpha_h}{\bar{v}(\bar{v}+\gamma_h)}\Gamma^4\bar{R}^4, \tag{36}$$

$$[\bar{e}]=\bar{c}_{\bar{v},\mathrm{mean}}(\bar{T}-\Gamma^2\bar{R}^2)+\frac{2\alpha_h}{\gamma_h}\Gamma^2\bar{R}^2\ln(1+\gamma_h)+\frac{2\alpha_h}{\gamma_h}\frac{\Gamma^4\bar{R}^4}{\bar{T}}\ln\left(\frac{\bar{v}}{\bar{v}+\gamma_h}\right), \tag{37}$$

$$[\bar{e}_{\bar{R}}]=\bar{c}_{\bar{v},\mathrm{mean}}(\bar{T}_{\bar{R}}-2\Gamma^2\bar{R}-2\Gamma\Gamma_{\bar{R}}\bar{R}^2)+\frac{4\alpha_h}{\gamma_h}\Gamma^2\bar{R}^2\ln(1+\gamma_h)\times\left(\frac{\Gamma_{\bar{R}}}{\Gamma}+\frac{1}{\bar{R}}\right)+\frac{2\alpha_h}{\gamma_h}\frac{\Gamma^4\bar{R}^4}{\bar{T}}\ln\left(\frac{\bar{v}}{\bar{v}+\gamma_h}\right)\times\left(4\frac{\Gamma_{\bar{R}}}{\Gamma}+\frac{4}{\bar{R}}-\frac{\bar{T}_{\bar{R}}}{\bar{T}}+\frac{\gamma_h\bar{v}_{\bar{R}}}{\bar{v}(\bar{v}+\gamma_h)}\frac{1}{\ln(\bar{v}/(\bar{v}+\gamma_h))}\right), \tag{38}$$

$$[\bar{e}_{\bar{x}}]=\bar{c}_{\bar{v},\mathrm{mean}}(\bar{T}_{\bar{x}})+\frac{2\alpha_h}{\gamma_h}\Gamma^4\bar{R}^4\left[-\frac{\bar{T}_{\bar{x}}}{\bar{T}^2}\ln\left(\frac{\bar{v}}{\bar{v}+\gamma_h}\right)+\frac{1}{\bar{T}}\frac{\gamma_h\bar{v}_{\bar{x}}}{\bar{v}(\bar{v}+\gamma_h)}\right]. \tag{39}$$

Expanding the variables $\bar{v}$, $\bar{u}$, $\bar{p}$, $\bar{e}$, $\bar{T}$, $\bar{q}$, $\bar{W}$, $\bar{B}$, and Γ in the form of an asymptotic power series in $\bar{R}$, the first terms of these equations, i.e., $\bar{v}_0$, $\bar{u}_0$, $\bar{p}_0$, $\bar{e}_0$, $\bar{T}_0$, $\bar{q}_0$, $\bar{W}_0$, $\bar{B}_0$, and Γ_0, satisfy a system of ordinary differential equations whose solution depends only on $\bar{x}$ $(=\bar{r}/\bar{R})$ referred to as "zero-order solution." This solution shows that, in the initial stage, we have a self-similar solution. This important result which resolves the difficulty associated with the initial singularities can indeed be justified by dimensional reasonings. $\bar{E}/\rho_0$ has the kinematic dimension of $[L^4/T^2]$ which is the square of the kinematic dimensions of viscosity μ/ρ_0 and thermal diffusivity $\kappa/(\rho_0 R^*)$. In the initial stage defined by $r\ll L$, the parameter L is irrelevant. Since there is no other length or time scale in the initial stage, dimensional considerations demand that the shock front must grow as $(\bar{E}/\rho_0)^{1/4}t^{1/2}$ and the shock speed must vary as $(\bar{E}/\rho_0)^{1/4}t^{-1/2}$.

The ODE system governing the zero-order solution can be deduced from the above differential system by setting

$\bar{R}=0$ and assuming the $\bar{R}$-derivative terms bounded. It is solved by the "prediction-evaluation-correction-evaluation" procedure (PECE) [8]. In this paper, we use the fourth-order predictor–corrector methods such as the Adams–Bashforth–Moulton pair. In the above calculations the values of the variables $\bar{v}$, $\bar{T}$, and Γ (also $\bar{v}_0$, $\bar{T}_0$, and Γ_0) at $x=0$ are unknown. The shooting methods [12, 13] combined with the PECE method are used to estimate these values. Once the zeroth-order solution is obtained, it may be continued for $\bar{R}>0$ by approximating the $\bar{R}$-derivatives in the governing differential system by backward Euler's differences.

We may compute the flow fields for a few time steps starting from $t=0$ ($\bar{R}=0$). In reality, however, there are difficulties with computational instability of the simple shooting methods. First, for the solution $y(x, s)$ of the initial-valued problem $y'=F(x, y)$, $y(a; s)=s$, one has

$$\| y(x; s_1)-y(x; s_2)\| \leqslant \|s_1-s_2\|\, e^{\beta|x-a|},$$

where s_1 and s_2 are two testing values. β is a parameter related to the given problem. Second, the Jacobian $\|D_y F(x, y)\|$ may be unbounded on $s=(x, y)|a\leqslant x\leqslant b$, $y\in\Re^n$. The above two difficulties restrict the value s to a small set M which as a rule is not a priori known [12]. In our case, we solve for the flow fields at $\bar{R}=0$, $\Delta\bar{R}$, $2\,\Delta\bar{R}$ (e.g., $\Delta\bar{R}=0.001$, the increment of the normalized shock radius $\bar{R}$), corresponding to the times $t=0$, Δt, $2\,\Delta t$, but cannot go further. The implicit donor-cell finite difference method will be used later to solve the flow fields as time evolves. Nevertheless, these initial solutions are essential for continuing the solution by the finite difference method, since $\bar{R}=0$ is a singular point of the governing differential system.

4. RESULTS FOR THE INITIAL STAGE

Isobutane C_4H_{10} at 20°C and 1 atm is a superheated liquid. It is used as a testing medium irradiated by neutrons at 1.55 MeV equivalent to the energy distribution along the neutron track $\bar{E}_c=6.231812\ \mathrm{g\cdot cm/s^2}$. Experiments showed that this neutron energy is the threshold energy to form a bubble developing indefinitely. The initial density of isobutane at $T=20°C$, $\rho_0=0.557069\ \mathrm{g/cm^3}$, the gas constant $R^*=1.987\ \mathrm{cal/g\cdot mole\ K}$ or $R^*=0.1431\times$

TABLE I

Data Related to Deposited Energy $\bar{E}$

$\bar{E}$	dE/dy (g·cm/s²)	L (cm)	χ
$0.50\bar{E}c$	3.115906×10^{-3}	0.20600×10^{-5}	0.38084
$0.75\bar{E}c$	4.673859×10^{-3}	0.25229×10^{-5}	0.31096
$1.00\bar{E}c$	6.231812×10^{-3}	0.29132×10^{-5}	0.26930
$2.00\bar{E}c$	12.46362×10^{-3}	0.41199×10^{-5}	0.19043

TABLE II

Data Related to Deposited Energy $\bar{E}$

$\bar{E}$	$\bar{\mu}_G$	$\bar{\mu}_L$	$\bar{K}_G$	$\bar{K}_L$
$0.50\bar{E}c$	3.84163×10^{-3}	6.53035×10^{-2}	0.0780202	0.38085
$0.75\bar{E}c$	3.13684×10^{-3}	5.33230×10^{-2}	0.0637022	0.31096
$1.00\bar{E}c$	2.71644×10^{-3}	4.61765×10^{-2}	0.0551670	0.26930
$2.00\bar{E}c$	1.92081×10^{-3}	3.26518×10^{-2}	0.0390096	0.19042

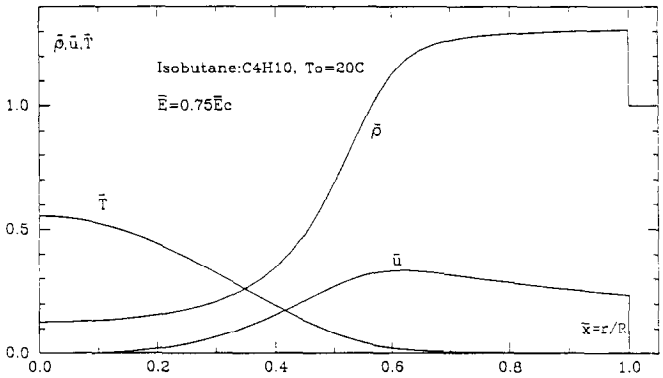

FIG. 1. Normalized flow fields in the initial stage.

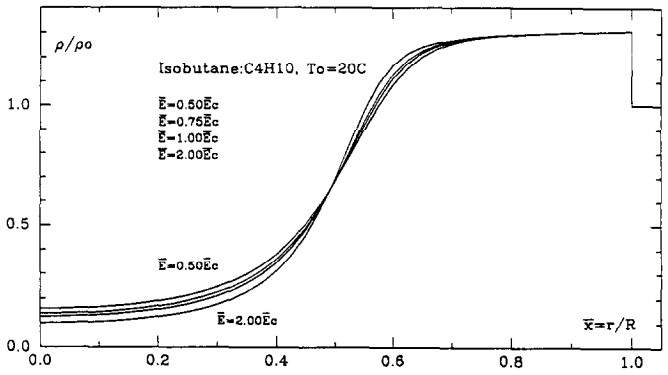

FIG. 2. Normalized density distributions with different input energy in the initial stage.

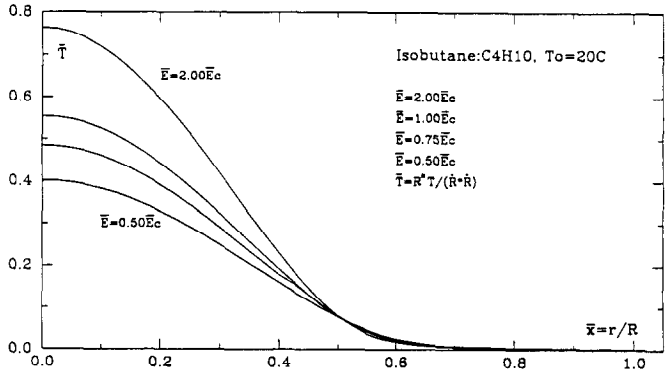

FIG. 3. Normalized temperature distributions with different input energy in the initial stage.

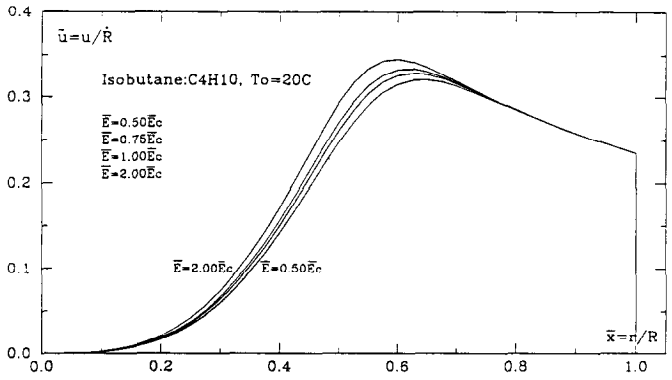

FIG. 4. Normalized velocity distributions with different input energy in the initial stage.

10^7 ergs/g K. The compressibility factor $\phi_0 = 0.00433494$. The parameters of the equation of state are $\alpha = 0.4280855$, $\beta = 0.0848836$, $\gamma = 1.0746463$. The other related parameters for different deposited energy $\bar{E}$ are listed in Tables I and II [9].

Figure 1 is the flow distribution at the initial stage for $\bar{E} = 0.75\bar{E}_c$. Figures 2, 3, and 4 are the density distribution, temperature distribution, and velocity distribution for different deposited energy $\bar{E}$. All the data are normalized values. The starting values $\bar{T}_0(0)$, $\bar{v}_0(0)$, Γ_0 are determined by the shooting method. The total number of nodes is 200; CPU time is about 80 s for each case on the Micro-VAX.

The above distributions can be roughly divided into two regions. For $\bar{x} < 0.7$, the variables change substantially, while in the outer region the variables change little.

The effect of viscosity on the solutions at this stage is found to be negligible, since the relative difference of the solutions between viscous cases and inviscid cases is within 0.005% for many examples studied. This result is in agreement with that of [7], which examined the effects of viscosity on the propagation of blast in an ideal gas.

5. SOLUTION IN THE PRE-BUBBLE FORMATION STAGE

The flow field in the initial stage has been computed for small values of $\bar{R}$ by a scaling transformation. However, the method of calculation becomes increasingly inefficient as the value of $\bar{R}$ increases. Hence, the implicit donor-cell finite difference method (FDM) [4, 6] is used to continue the solution beyond the initial stage. The results show that the implicit donor-cell FDM is efficient and accurate for the pre-bubble formation stage; however, difficulty arises when the density gradients become steep at the place where the phase change is about to occur.

The governing equations, i.e., Eqs. (16)–(20) are rewritten in conservation form for the application of the implicit donor-cell FDM,

$$\bar{\rho}_\tau + (\bar{\rho}\bar{w})_{\bar{x}} + \bar{\rho}\left(2 + \frac{\bar{w}}{\bar{x}}\right) = 0, \tag{40}$$

where subscripts τ and $\bar{x}$ signify the partial derivatives with respect to the indicated variables, and

$$(\bar{\rho}\bar{w})_\tau + \left(\bar{p} + \bar{\rho}\bar{w}^2 - \frac{4}{3}\Gamma\bar{\mu}\bar{z}\right)_{\bar{x}} + \bar{\rho}(\bar{w} + \bar{x})(\ln V_s)_\tau + \bar{\rho}\bar{w}\left(3 + \frac{\bar{w}}{\bar{x}}\right) + 2\Gamma\bar{y}\left(\frac{\bar{w}}{\bar{x}} + 1\right) = 0, \tag{41}$$

$$\left[\bar{\rho}\left(\bar{e} + \frac{1}{2}\bar{w}^2\right)\right]_\tau + \left[\bar{\rho}\bar{w}\left(\bar{e} + \frac{1}{2}\bar{w}^2\right) + \bar{p}\bar{w} - \Gamma q\frac{4}{3}\Gamma\bar{\mu}\bar{z}\bar{w}\right]_{\bar{x}} + \frac{1}{2}\bar{\rho}\bar{w}^2\left(4 + \frac{\bar{w}}{\bar{x}}\right) + (\bar{p} + \bar{\rho}\bar{e})\left(2 + \frac{\bar{w}}{\bar{x}}\right) + \bar{\rho}(2\bar{e} + (\bar{w} + \bar{x})\bar{w})[\ln V_s]_\tau - \Gamma\frac{\bar{q}}{\bar{x}} + \frac{4}{3}\Gamma\bar{\mu}\bar{z}\frac{\bar{w}}{\bar{x}} + \Gamma\left(\frac{\bar{w}}{\bar{x}} + 1\right) \times \left[\frac{4}{3}\bar{\mu}\bar{z} + 2\bar{w}\bar{y} - 4\bar{\mu}\left(\frac{\bar{w}}{\bar{x}} + 1\right)\right] = 0, \tag{42}$$

$$\bar{T}_{\bar{x}} = \bar{q}/\bar{\chi}, \tag{43}$$

where

$$\bar{w} = \bar{u} - \bar{x},$$

$$\bar{z} = \bar{w}_{\bar{x}} + \frac{\bar{w}}{\bar{x}} + 2, \qquad \bar{z}_{\bar{x}=0} = 0,$$

$$\bar{y} = \bar{\mu}_{\bar{x}},$$

$$[\,]_\tau = \frac{\partial}{\partial\tau}[\,] = \bar{R}\frac{\partial}{\partial\bar{R}}[\,]$$

and

$$\tau = \ln \bar{R}, \qquad \bar{R} = e^\tau.$$

Here, τ is the variable corresponding to the time.

In the above equations,

$$\bar{e} = \int_{\Gamma^2\bar{R}^2}^{T} \bar{c}_{\bar{v},\text{ideal}}\left(\frac{T_0\tau}{\Gamma^2\bar{R}^2}\right)d\tau + \frac{2\alpha_h}{\gamma_h}\Gamma^2\bar{R}^2\ln(1 + \gamma_h) + \frac{2\alpha_h}{\gamma_h}\frac{\Gamma^4\bar{R}^4}{\bar{T}}\ln\left(\frac{1}{1 + \bar{\rho}\gamma_h}\right) \tag{44}$$

and

$$\Gamma = \frac{1}{V_s\bar{R}} = \frac{1}{V_s e^\tau}. \tag{45}$$

The basic unknowns are $\bar{\rho}_i$, $\bar{u}_i$, and $\bar{T}_i$ $(i = 1, 2, ..., m)$ and the normalized shock speed V_s, where $\bar{\rho}_i$, $\bar{u}_i$, and $\bar{T}_i$ denote

respectively the non-dimensionalized density, velocity, and temperature at the ith spatial node in a finite difference grid having a total of m nodes. The specific internal energy $\bar{e}$ can be described as a function of $\bar{\rho}_i$, $\bar{u}_i$, and $\bar{T}_i$ $(i=1, 2, ..., m)$, using Simpson's integral algorithm. Equations (40)–(44), together with the global energy equation

$$\Gamma^2=\left(\frac{1}{V_s e^{\tau}}\right)^2=2\int_0^1 x\,dx\,\frac{(\bar{e}+\bar{u}^2)}{2}\,\bar{\rho}, \tag{46}$$

form a system of equations whose solution gives the flow field in the pre-bubble formation stage.

The above governing equations can be solved by the implicit donor-cell FDM through an iteration process such as the well-known Newton iteration method. In the Newton iteration method, the main task lies in forming the Jacobian. A reasonable error tolerance is given to control the iteration. Since it is important to have a good first guess in solving the nonlinear algebraic system, we propose to obtain a reasonable first guess by extrapolating the results obtained in the three previous time steps. The usual method of using an explicit formulation with time derivatives approximated by forward differences breaks down at $\bar{R}=0$ and yields poor results when $\bar{R}$ is small. On the other hand, if the initial information (the first three time steps) is supplied by the scaling transformation solutions, the resulting iteration is found to be $3\sim4$ times faster than using the forward Euler's formula for calculating the first guesses.

As regards the boundary conditions at $\bar{x}=1$, an imaginary point, i.e., the $(m+1)$th point, is introduced (Fig. 5), where m is the total number of nodes. The flow is continued beyond $\bar{x}=1$ as though there were no discontinuity there and the values of $\bar{\rho}_{m+1}$, $\bar{u}_{m+1}$, and $\bar{T}_{m+1}$ at the imaginary point are determined by insisting that the jump conditions at $\bar{x}=1$ are satisfied (cf. Eqs. (31)). No imaginary point is introduced at $\bar{x}=0$.

It should be noted again that the fluid ahead of the shock front is assumed to be inviscid and the imposition of the three boundary conditions at the shock $\bar{x}=1$ implies that we have purposefully suppressed the possibility of solving the structure of the shock layer and the rapid transition therein. This should not be taken as meaning the thickness of shock wave is negligible compared with all relevant length scales in the problem. While it is indeed negligible when compared with the shock radius if $\bar{E}\gg\rho\mu^2$, it is nevertheless of the order of the radius of the critical size bubble, as one of the reviewers of this paper has noted. We believe our model should correctly predict the formation, growth, and/or collapse of the bubble, because the dynamics of bubble formation and motion depends on the net thermodynamics effects of the shock wave on the mediums which have been accounted for by imposing the appropriate boundary conditions at the shock and because when the bubble is formed, the shock wave is located so far away that its structure should have no effect on the growth and collapse phenomena that we are interested in.

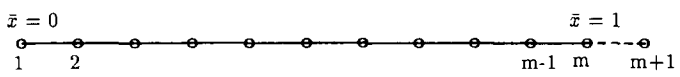

FIG. 5. The imaginary node $m+1$ at boundary $\bar{x}=1$.

6. RESULTS FOR THE PRE-BUBBLE FORMATION STAGE

Isobutane C_4H_{10} at 20°C and the deposited energy $\bar{E}=1.0\bar{E}_c$ is taken as an example. The related data are shown in Tables I and II. The total number of nodes m is 200.

The dimensionless shock velocity V_s $(=\dot{R}/(R^*T_0)^{1/2})$ as a function of $\bar{R}$ can be computed immediately from Eq. (15), since Γ at each $\bar{R}$ has been determined in the computation. This is shown in Fig. 6.

The dimensionless shock radius $\bar{R}$ $(=R/L)$ as a function of the dimensionless time $\bar{t}$ $(=t(R^*T_0)^{1/2}/L)$ can be calculated from Eq. (14), and this is shown in Fig. 7. Note that $\bar{R}$ is a monotone increasing function of time $\bar{t}$ in the initial stage. Indeed, $\bar{R}$ has been adopted as the "time variable."

The evolution of the thermal spike is shown in Fig. 8, where $\bar{T}$ is plotted against $\bar{x}$ at different values of $\bar{R}$. It may be recast in a more easily visualized form. In Fig. 9, the temperature distribution $T(r, t)$ at different time t is plotted as T/T_0 vs r/L at various $\bar{t}=tu_g/L$, where $u_g=(R^*T_0)^{1/2}$.

At a given instant $\bar{R}$, there is a pressure $\bar{p}$ as well as a temperature $\bar{T}$ at each point $\bar{x}$ within the shock enclosure. This fact is depicted in Fig. 10, where a plot of $\bar{p}$ vs $\bar{T}$ at different values of $\bar{R}$'s is given. The location at which the particular $\bar{p}$ and $\bar{T}$ at the instant $\bar{R}$ occurs can be indicated on each of the $\bar{p}\bar{T}$-curves. Indeed, the broken lines are the lines at constant $\bar{x}$'s. Also shown in the figure are the critical pressure and temperature. To give a physical interpretation to this graph, we observe that as time increases, the $\bar{p}\bar{T}$-curve

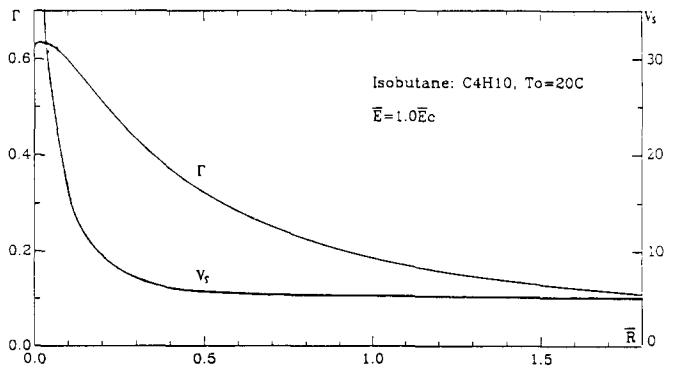

FIG. 6. Γ, V_s vs $\bar{R}$ in the initial and pre-bubble formation stages.

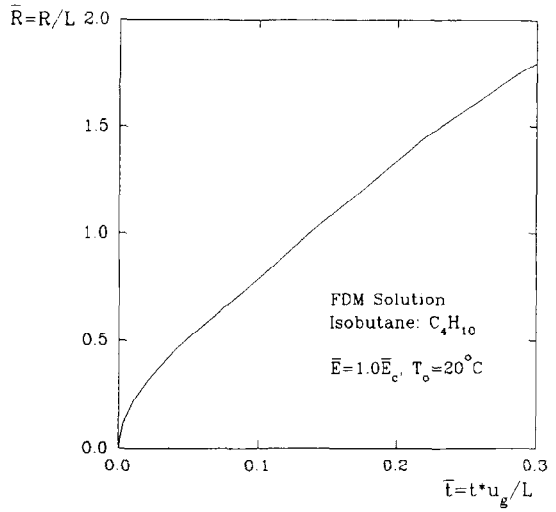

FIG. 7. The relation between the normalized shock radius $\bar{R}$ and time $\bar{t}$.

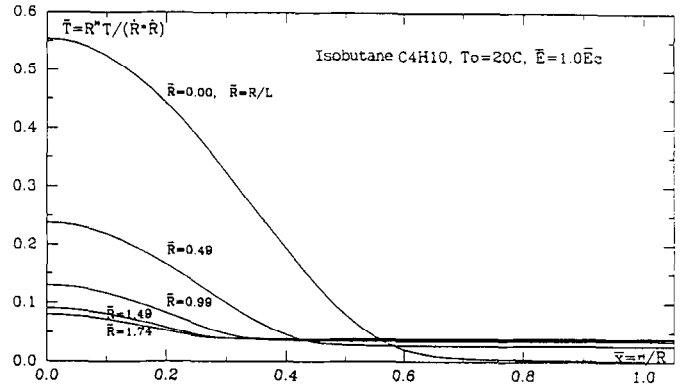

FIG. 8. Temperature distributions normalized by $\bar{T} = R^*T/(\dot{R} * \ddot{R})$ and $\bar{x} = r/R$ as $\bar{R} \leqslant 1.74$.

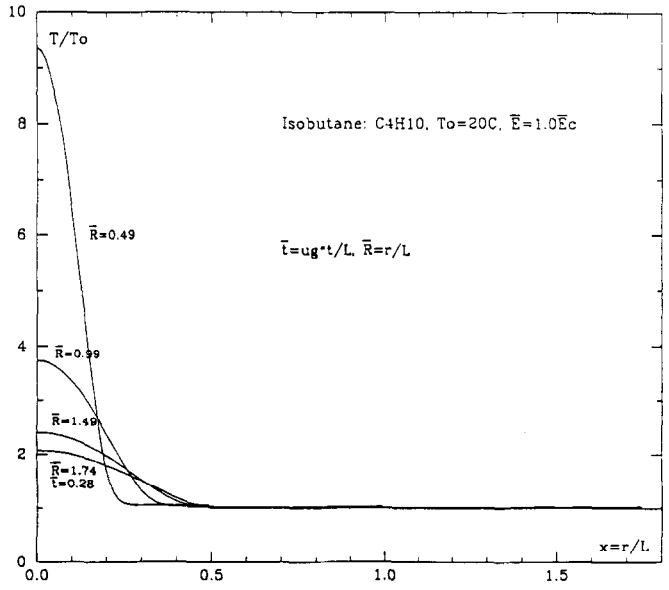

FIG. 9. Temperature distributions normalized by $\bar{T} = T/T_0$ and $x = r/L$ as $\bar{R} \leqslant 1.74$.

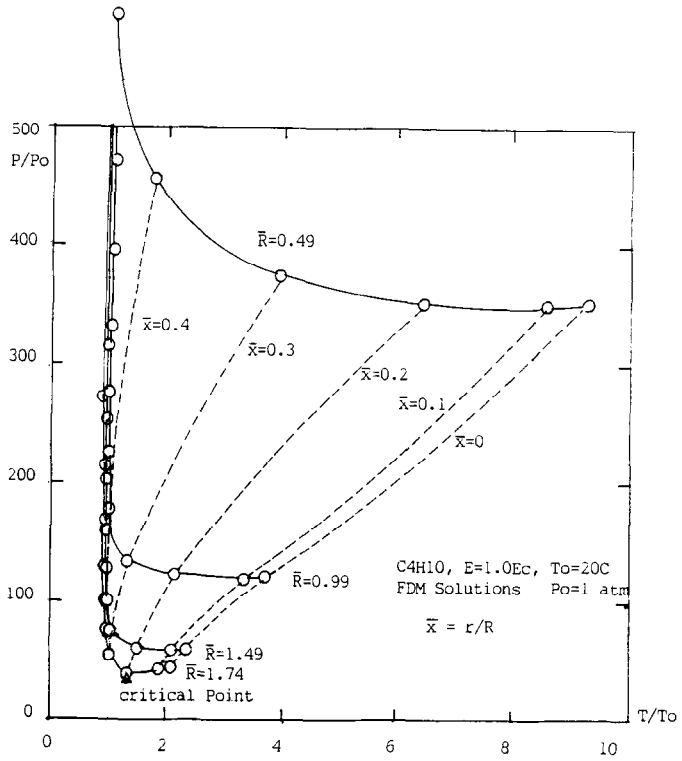

FIG. 10. $\bar{p} - \bar{T}$ relation in the pre-bubble formation stage.

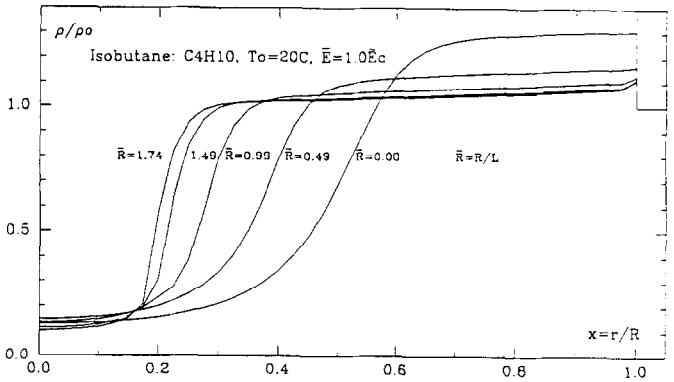

FIG. 11. Density distributions normalized by $\bar{\rho} = \rho/\rho_0$ and $x = r/R$ as $\bar{R} \leqslant 1.74$.

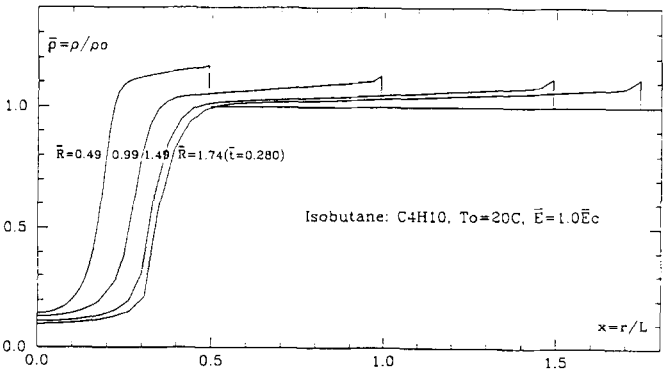

FIG. 12. Density distribution normalized by $\bar{\rho} = \rho/\rho_0$ and $x = r/L$ as $\bar{R} \leqslant 1.74$.

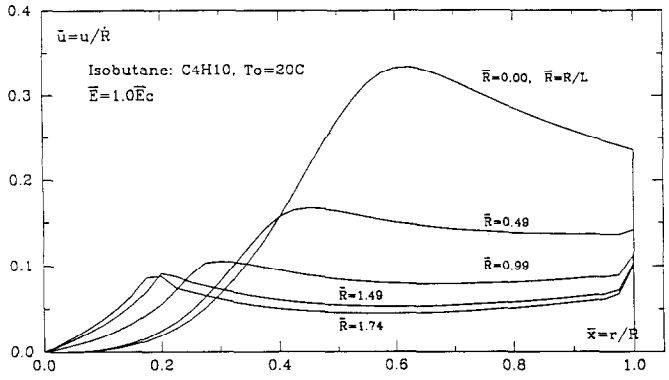

FIG. 13. Velocity distributions normalized by $\bar{u} = u/\dot{R}$ and $\bar{x} = r/R$ as $\bar{R} \leqslant 1.74$.

sweeps from a small value of $\bar{R}$ (e.g., $\bar{R} = 0.49$) to larger values of the time variable $\bar{R}$. It is clear that nowhere can a vapor–liquid interface form in the medium until the $\bar{p}\bar{T}$-curve crosses the critical point.

The evolution of the density field is shown in Figs. 11 and 12. It shows that there is a gradual steepening of the density gradient even prior to the formation of the vapor–liquid interface. The velocity distribution is shown in Figs. 13 and 14. The apparent "infinite" curvature exhibited by the velocity profiles at the shock front (where $\bar{x} = 1$) is, of course, a consequence of our deliberate attempt to avoid resolving the extremely thin shock layer. The CPU times to calculate the pre-bubble stage are about 30 min on the Micro-VAX.

When phase change is about to occur, the density gradient becomes rather steep somewhere. Since the location of such a steep gradient changes with time, it is obvious that an adaptive method of solution is required. For this reason, the above method of solution, using a fixed grid, is not suitable in the post-interface formation stage.

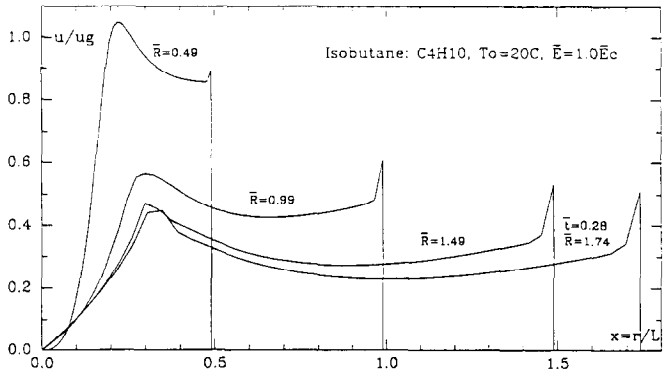

FIG. 14. Velocity distributions normalized by $\bar{u} = u/u_g$ and $\bar{x} = r/L$ as $\bar{R} \leqslant 1.74$.

7. SUMMARY

The radiation-induced cavitation process is studied by dynamic theory and numerical analysis. The scaling transformation is successfully used to overcome the singularity difficulty and to establish the initial conditions for later calculation. The implicit donor-cell finite difference method is introduced to compute the solution for short times to improve the computation efficiency. The details of the flow fields are solved by the above methods in the initial stage and the pre-bubble formation stage. The density gradient in the medium stage increases with time evolution. The simple non-adaptive finite difference method cannot be expected to give satisfactory answers in describing the formation and growth of the vapor–liquid interface. The adaptive computational methods will be used in part II to solve the flow fields for the interface formation and post-interface formation stages. General conclusions will be made in part II of this paper.

ACKNOWLEDGMENTS

This research work is supported in part by the U.S. Department of Energy under Contract No. DE-AC02-81EV10673-A000 and DE-FG02-87ER60500, and in part by the U.S. ONR under Contract No. N00014-82-K-0184. We wish to thank Professors Tony Chan, William Gropp, David Keyes, Mitchell Smooke, and Dr. John Mengle for their valuable discussions.

REFERENCES

1. R. E. Apfel, U.S. Patent No. 4, 143, 274 (1979).
2. R. E. Apfel, *Nucl. Instrum. Methods* **162**, 603 (1979).
3. R. E. Apfel, B. T. Chu, and J. Mengel, *Appl. Sci. Res.* **38**, 117 (1982).
4. C. W. Hirt, *J. Comput. Phys.* **2**, 339 (1968).
5. C. Horvath and H. J. Lin, *Can. J. Chem. Eng.* **55**, 450 (1977).
6. K. Y. Huh, M. W. Golay, and V. P. Manno, *J. Comput. Phys.* **63**, 201 (1986).
7. M. M. Kamel, H. A. Khater, H. G. Siefien, N. M. Rafat, and A. K. Oppenheim, *Acta Astronaut.* **4**, 425 (1977).
8. J. D. Lambert, *Computational Methods in Ordinary Differential Equations* (Arrowsmith, Bristol, UK, 1973), p. 85.
9. R. C. Reid, I. M. Prausnitz, and T. K. Sherwood, *The Properties of Gases and Liquids*, 3rd ed. (McGraw-Hill, New York, 1977).
10. S. C. Roy and R. E. Apfel, *Nucl. Instrum. Methods* **219**, 582 (1984).
11. F. Seitz, *Phys. Fluids* **1**, 2 (1958).
12. J. Store and R. Bulirsch, *Introduction to Numerical Analysis* (Springer-Verlag, New York, 1980), p. 469.
13. G. Witmer, V. Balakotaiah, and D. Luss, *J. Comput. Phys.* **65**, 244 (1986).
14. Y. Y. Sun, B. T. Chu, and R. E. Apfel, "*Cavitation and Multiphase Flow Forum–50th Annu. ASME Conference, Cincinnati, Ohio, 1987*," edited by O. Furuya, p. 45.